

## Flying through polytropes

W. Dean Pesnell

Citation: [Am. J. Phys.](#) **84**, (2016); doi: 10.1119/1.4939574

View online: <http://dx.doi.org/10.1119/1.4939574>

View Table of Contents: <http://aapt.scitation.org/toc/ajp/84/3>

Published by the [American Association of Physics Teachers](#)

---

---

# Flying through polytropes

W. Dean Pesnell<sup>a)</sup>

NASA, Goddard Space Flight Center, Greenbelt, Maryland, 20771

(Received 12 June 2015; accepted 16 December 2015)

Dropping objects into a tunnel bored through Earth has been used to visualize simple harmonic motion for many years, and even imagined for use as rapid transport systems. Unlike previous studies that assumed a constant density Earth, here we calculate the fall-through time of polytropes, models of Earth's interior where the pressure varies as a power of the density. This means the fall-through time can be calculated as the *central condensation* varies from one to large within the family of polytropes. Having a family of models, rather than a single model, helps to explore the properties of planets and stars. Comparing the family of phase space solutions shows that the fall-through time and velocity approach the limit of radial free-fall onto a point mass as the central condensation increases. More condensed models give higher maximum velocities but do not have the right global properties for Earth. The angular distance one can travel along the surface is calculated as a brachistochrone (path of least time) tunnel that is a function of the depth to which the tunnel is bored. We also show that completely degenerate objects, simple models of white dwarf stars supported by completely degenerate electrons, have sizes similar to Earth but their much higher masses mean a much larger gravitational strength and a shorter fall-through time. Numerical integrations of the equations describing polytropes and completely degenerate objects are used to generate the initial models. Analytic solutions and numerical integration of the equations of motion are used to calculate the fall-through time for each model, and numerical integrations with analytic approximations at the boundaries are used to calculate the brachistochrones in the polytropes. Scaling relationships are provided to help use these results in other planets and stars. © 2016 American Association of Physics Teachers.

[<http://dx.doi.org/10.1119/1.4939574>]

## I. INTRODUCTION

A well-known problem in physics is to calculate how long it would take for an object to fall through a tunnel bored through the center of Earth and emerge from the other side, ready to be plucked by a waiting confederate.<sup>1</sup> This problem has been discussed in many contexts,<sup>2</sup> including the classic book on special and general relativity by Misner *et al.*<sup>3</sup> The problem can be generalized to tunnels from one point on the surface of Earth to another, that follow brachistochrones, or paths of least time.<sup>4</sup>

A recent paper comparing the fall-through time of a constant density model of Earth with a more realistic model revealed a shorter fall-through time.<sup>5</sup> This difference was attributed to the higher *central condensation*, or ratio of central mass density to mean density, of the more realistic model. One way to test this conclusion is by calculating the fall-through time as a function of central condensation. Polytropes—models of planets or stars where the pressure varies as a power of the density (described in Sec. II)—form a class of models that probes almost the entire range of central condensation. These models are characterized by a polytropic index ( $n$ ) that varies from 0 (constant density) to 5 (infinite central condensation but finite central density). In the limit as  $n \rightarrow 5$ , the model has an enormous concentration of mass at the center and behaves more like a point mass than an extended planet.

Polytropes can be a more accurate model of Earth's interior, albeit without discontinuities, so the fall-through time was calculated for polytropes matched to the mass and radius of Earth. The result is a smooth increase in the fall velocity that approaches the Keplerian radial infall velocity<sup>6</sup> as  $n \rightarrow 5$ . This also means that the fall-through time has a lower

limit of about 29.83 min, the radial infall time of an object starting one Earth radius from a point mass with the mass equal to that of Earth.

The central condensation also affects the brachistochrones, or paths of least time, calculated for a path joining two points on the surface and tangent to a radius within the model. For a given tangent radius, the angular distance traversed by a brachistochrone decreases as the central condensation increases.

Klotz<sup>7</sup> examined the fall-through times and brachistochrones for simple planetary models where the mass density varied as a power law of the radius. Although the results are similar to those presented here, such models are less appropriate to planetary interiors than are polytropes. For example, a density that varies as  $r^{-2}$  ( $\alpha = -1$  in the notation of Klotz) approximates the coma of a comet, but only in the presence of an expansion velocity.<sup>8</sup>

Brachistochrones are described for motion in the central field of a point mass in Sec. 606 of Routh.<sup>9</sup> A more recent update shows there are no brachistochrone trajectories with a particular angular range as the trajectory nears the origin.<sup>10</sup> Polytropes will be shown to have a similar behavior as  $n \rightarrow 5$ , but the brachistochrone approaches a straight tunnel as the trajectory comes closer to the origin and passes the maximum in the gravitational field strength.

The fall-through time for models using the completely degenerate equation of state (EOS) is also examined to show that the velocities can become relativistic as the dropped object passes through the core. These completely degenerate objects are models of the cores of gas giant planets and white dwarfs.

We will first describe polytropes and why they are useful in planetary models. Polytropic models with the radius and

mass of Earth are used to calculate how the fall-through time varies with  $n$ . Brachistochrones are introduced next and calculated for several values of  $n$  and turning point distance. Both of these calculations identify the polytropic function as the gravitational potential to simplify the solutions. We will conclude by applying the fall-through time analysis to completely degenerate models that are simple models of white dwarfs.

## II. POLYTROPES

Conditions deep inside planets have not been directly measured. They can be inferred from the velocities of waves generated by earthquakes moving through the interior. They can also be estimated from models that satisfy the known global quantities, such as mass and radius, and the conservation equations from the center to the surface.

Polytropes are models of stars and planets that use the equation of state  $P = K\rho^{1+1/n}$  to derive hydrostatic configurations of the pressure  $P$  and mass density  $\rho$ . The polytropic equation of state (EOS) relates  $P$  to  $\rho$  with a constant  $K$  and the polytropic index  $n$ . The value of  $K$  is related to the entropy of the gas. Polytropes were used to estimate the central conditions of stars. For example, the standard model of the Sun advocated by Eddington<sup>11</sup> is an  $n=3$  polytrope. The central temperature of the Sun was estimated as 20 MK with this model (Cox and Giuli, Sec. 23.2),<sup>12</sup> which was an important step to realizing nuclear fusion provided the thermal energy that supports normal stars. Any gravitating body, where this simple EOS can be used, can be understood as a polytrope. Accurate models of planet interiors have a more complicated EOS than polytropic.<sup>13,14</sup> In particular, partial degeneracy, which this simple EOS does not include, can be important in the cores of gas giant planets. But polytropes may have a more accurate variation of gravity with radius than the constant density model used for the fall-through time calculation.<sup>15–17</sup>

Following the derivation in Chapter 4 of Chandrasekhar,<sup>18</sup> combining the equation of spherical hydrostatic equilibrium

$$\frac{1}{\rho} \frac{dP}{dr} = -\frac{GM(r)}{r^2}, \quad (1)$$

which represents the balance of the pressure gradient and gravitational acceleration, with the equation of mass conservation

$$\frac{dM(r)}{dr} = 4\pi r^2 \rho \quad (2)$$

yields a Poisson equation for the internal gravitational potential that links the run of pressure and density within the model

$$\frac{1}{r^2} \frac{d}{dr} \left( \frac{r^2 dP}{\rho dr} \right) = -4\pi G \rho. \quad (3)$$

The polytropic EOS provides another relationship between  $P$  and  $\rho$ . The polytropic function  $\theta$  is introduced as  $\rho = \rho_c \theta^n$ , where  $\rho_c$  is the mass density at the center of the model, and a new independent variable defined by  $r = \epsilon \xi$ , where

$$\epsilon^2 = \frac{(n+1)K}{4\pi G} \rho_c^{1/n-1} \quad (4)$$

is found by combining the scaling factors of the quantities in Eq. (4). The result is the Lane-Emden equation

$$\frac{1}{\xi^2} \frac{d}{d\xi} \left( \xi^2 \frac{d\theta}{d\xi} \right) = -\theta^n. \quad (5)$$

A solution of Eq. (5) requires two boundary conditions, which are chosen to be  $\theta=1$  and  $d\theta/d\xi=0$  at the center of the model ( $\xi=0$ ). The surface of the model ( $\xi_0$ ) is at the first zero of  $\theta$ . Physical solutions for  $\theta$  exist for  $0 \leq n < 5$ .

Several global quantities come from polytropic models. One is the central condensation of a model, the ratio of the central density to the mean density, which is related to the surface conditions by

$$\frac{\rho_c}{\bar{\rho}} = -\frac{\xi_0}{3} \left( \frac{d\theta}{d\xi} \Big|_0 \right)^{-1} \quad (6)$$

evaluated at  $\xi_0$ . Another is the central pressure  $P_c = 4\pi G(\epsilon \rho_c)^2/(1+n)$ . Values for the central condensation and  $P_c$  are listed in Table I for the polytropes used here. The physical radius of the model is  $r = \epsilon \xi$ .

Another useful relationship is the mass within a sphere of radius  $\xi$

$$M(\xi) = -4\pi \epsilon^3 \rho_c \xi^2 \frac{d\theta}{d\xi}, \quad (7)$$

which, when evaluated at the surface, gives the mass of the polytrope

$$M = -4\pi \epsilon^3 \rho_c \xi_0^2 \frac{d\theta}{d\xi} \Big|_{\xi_0}. \quad (8)$$

The radial gravitational acceleration that is needed for the fall-through time calculation comes from Eq. (7) as

$$g = \frac{GM(r)}{r^2} = -4\pi G \epsilon \rho_c \frac{d\theta}{d\xi}. \quad (9)$$

Global quantities of polytropes can be matched to an observed planet or star, which can then be used to estimate the central conditions of them. Properties within sets of

Table I. Properties of Earth-like polytropes.

$n$	$\xi_0$	$\rho_c/\bar{\rho}$	$P_c$ (dyn/cm <sup>2</sup> )	$T_0$ (min)	$v_{\max}$ (km/s)
0	2.449	1	$1.72 \times 10^{12}$	42.20	7.91
PREM	—	2.36	$3.64 \times 10^{12}$	38.13	8
0.715	2.908	2.36	$3.97 \times 10^{12}$	36.96	10.2
1	3.141	3.29	$5.67 \times 10^{12}$	35.64	11.2
1.5	3.653	5.99	$1.11 \times 10^{12}$	34.0	13.0
2	4.352	11.4	$2.37 \times 10^{13}$	32.72	15.0
3	6.896	54.2	$2.60 \times 10^{14}$	31.13	20.7
3.5	9.536	153	$5.91 \times 10^{14}$	30.62	25.1
4	14.96	622	$3.58 \times 10^{15}$	30.24	32.3
4.5	31.83	$6.19 \times 10^3$	$7.11 \times 10^{16}$	29.98	47.9
4.75	66.40	$5.66 \times 10^4$	$1.31 \times 10^{18}$	29.89	69.4
Radial infall to point mass					29.83
					—

planets can also be compared, as in the case of an ensemble of similar objects that will group together along the mass-radius relationship. For polytropes, this is derived by eliminating  $\rho_c$  between the total mass in Eq. (8) and the outer radius  $R = \epsilon\xi_0$  as

$$R^{(3-n)/n} M^{(1-n)/n} \propto K. \quad (10)$$

Starting from smaller masses (like the terrestrial planets) and moving to masses larger than Jupiter, there are four interesting regions for planets and stars. The first is for  $n=0$ , which are homogeneous spheres where the radius increases with increasing mass ( $R \propto M^{1/3}$ ). The second is for  $n=1$ , which is roughly consistent with the giant planets in our solar system ( $R \sim \text{constant}$ ). The third is for  $n=3/2$ , where the pressure is dominated by completely degenerate, non-relativistic electrons, and the radius decreases with increasing mass ( $R \propto M^{-1/3}$ ). This region is also the lowest value of  $n$  for which the model may be convectively stable. Lastly we have  $n=3$ , which is the basis of the Eddington Standard Model of the Sun. The mass-radius relationship shows that the mass of the model is independent of the radius.

Many extrasolar planets have been observed by the Kepler satellite.<sup>19</sup> These planets have shown that the mass-radius relation is more complicated than the first three divisions listed here,<sup>20</sup> and thus requiring the development of more accurate models of gas-giant planets.<sup>13</sup> But polytropes are a good place to start developing an understanding of the internal structure of planets and stars. The numerical techniques used to integrate the conservation equations can be developed for the simpler polytropes and then applied to the more accurate models.

### III. EARTH MODEL

By providing two of the three quantities: mass, radius, or average density, a physical model of a star or planet can be built from a polytrope with a value of  $n$  between 0 and 5. This freedom comes from not knowing  $K$  in the equation of state. If  $K$  were known then one could only specify one of these quantities and the others would be calculated. Consistent values for all three quantities are available for Earth:  $M_\oplus = 5.972 \times 10^{24} \text{ kg}$ ,  $\bar{\rho} = 5.514 \text{ g cm}^{-3}$ ,  $R_\oplus = 6371 \text{ km}$ .

The Preliminary Reference Earth Model (PREM) is a global reference originally published by Dziewonski and Anderson.<sup>21</sup> In addition to containing the discontinuities and transitions that had been found before, the density distribution of the PREM is consistent with the eigenfrequencies observed in seismometers after a very large earthquake. The PREM<sup>22</sup> data have the central pressure of Earth as 364 GPa, or  $3.64 \times 10^{12} \text{ dyn cm}^{-2}$ , the central temperature between 5000 and 6000 K, and a central density of  $13 \text{ g cm}^{-3}$ . This means that the ratio of the central to average density is 2.36, indicating that a polytrope of  $n=1$  is already too centrally condensed;  $n=0.715$  is a better fit to the PREM data.

### IV. FALL-THROUGH TIME

Polytrope models for several values of  $n$  were integrated with the Runge-Kutta shooting method described by Pesnell.<sup>23,24</sup> A value is chosen for  $\xi_0$  and the Lane-Emden equation [Eq. (5)] is integrated from  $\xi=0$  towards the surface until  $\theta$  changes sign. A Newton's method is then used to converge the value of  $\xi_0$ . Values for  $\xi_0$ ,  $\rho_c/\bar{\rho}$ , and the central

pressure of an Earth-matched model for each  $n$  are listed in Table I. The variation of  $\rho/\rho_c$  and  $g/g_{\max}$  with normalized radius for several values of  $n$  are shown in Fig. 1. As  $n$  increases from 0 to 5, the model becomes more centrally condensed and the location of the maximum in the gravitational field strength moves inward.

A tunnel connecting two antipodal points is imagined to be bored through the center of the model (Fig. 2). The gravitational field strength in the model [ $g$  in Eq. (9)] can be used in the equations of motion ( $dr/dt=v$  and  $dv/dt=-g$ ) to calculate the time  $T_0$  it takes to fall through the tunnel and the maximum velocity  $v_{\max}$  reached. While numerical integration of the equations will be described below,  $v_{\max}$  can be calculated from  $\theta$ . This anticipates identifying  $\theta$  as a gravitational potential in the integration of the brachistochrones in Sec. V below.

We start with the radial acceleration equation

$$\frac{dv}{dt} = \frac{dv}{dr} \frac{dr}{dt} = -g, \quad (11)$$

which can be integrated with respect to radius on the left side to give the specific kinetic energy. Using Eq. (9) and transforming to polytropic coordinates, the right side integrates to give the gravitation potential. We find

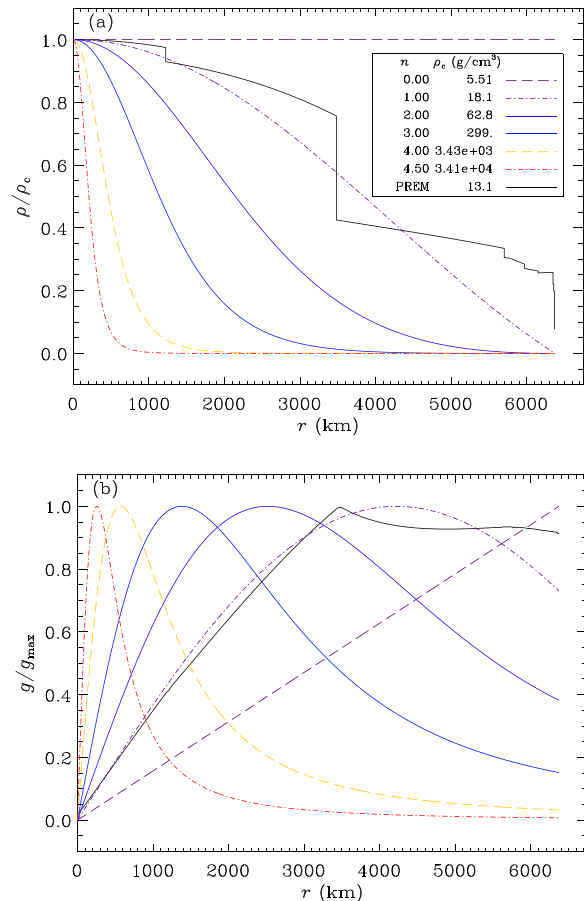


Fig. 1. The relative density (a) and gravitational field strength (b) variations in selected polytropes and the PREM model. Polytropes have a more centrally concentrated density as  $n$  increases. The gravitational field strength also becomes more centrally condensed as  $n$  increases; this makes sense as  $g$  is proportional to the derivative of  $\theta$  [Eq. (9)] and the more centrally condensed a model becomes the steeper the slope near the center of the model.

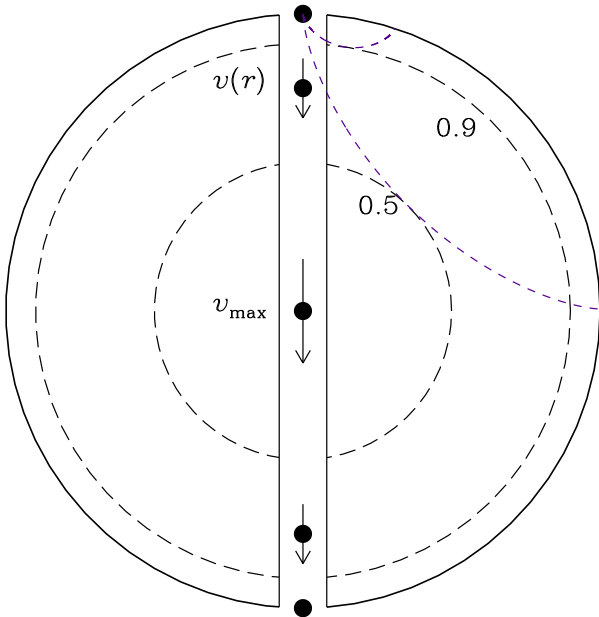


Fig. 2. An illustration of the calculation of the fall-through time experiment. The projectile falls from the top of the planet to the bottom. The length of the vector indicates the velocity. The dashed circles show two of the inner radii of the brachistochrone trajectories for an object released at the top of the planet. The other dashed curves show two brachistochrones that start from the same initial position and move through the interior, becoming tangent to the inner radius of the trajectory, and then returning to the surface. The inner radii of the two plotted trajectories are 0.5 and 0.9 times the outer radius.

$$\frac{1}{2}v^2(r) = - \int_r^R g dr \Rightarrow \frac{1}{2}v^2(\xi) = 4\pi G e^2 \rho_c \theta(\xi), \quad (12)$$

where the velocity and  $\theta$  are both 0 at the surface. The velocity of a projectile falling through the tunnel is

$$v(\xi) = \frac{R}{\xi_0} \sqrt{8\pi G \rho_c \theta(\xi)}, \quad (13)$$

and the maximum velocity is  $v_{\max} = v(0) = (R/\xi_0) \sqrt{8\pi G \rho_c}$ , since  $\theta(0) = 1$  at the center. The fall-through time can now be calculated as twice the time to move from the surface to the center with this velocity profile

$$T_0 = 2 \int_0^R \frac{dr}{v(r)} = \frac{1}{\sqrt{2\pi G \rho_c}} \int_0^{\xi_0} \frac{d\xi}{\sqrt{\theta(\xi)}}. \quad (14)$$

Usually, this time must be numerically calculated but it can be analytically evaluated for  $n=0$ , and the model matched to Earth to yield  $T_0 = 42.17$  min.

The fall velocity and position of the projectile as a function of time were also calculated by numerically integrating the equations of motion for a projectile starting from rest at the surface and moving through the tunnel (Fig. 2). A 4th-order Runge-Kutta method was used for this integration. The time  $T_f$  it takes to reach the center was calculated, and fall-through time, or how long it takes to reach the other side of the model, is  $T_0 = 2T_f$ . The maximum velocity is reported as  $v_{\max}$ .

Values of  $T_0$  and  $v_{\max}$  from this numerical integration are listed for each polytropic model in Table I. The second line

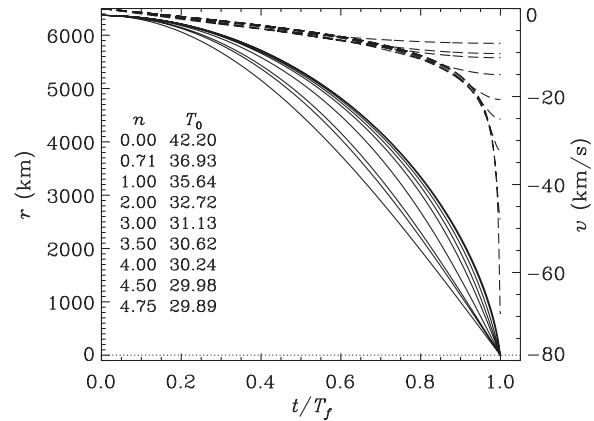


Fig. 3. The change in radial position (solid) and velocity (dashed) as functions of time for an object falling through Earth. The time has been normalized to the time it takes to reach the center of the model. Values of  $n$  and  $T_0$  are shown in the legend. The dashed curves track  $n$  from the top down while the solid curves track  $n$  from the bottom up.

of Table I shows the results of the PREM model calculated by Klotz.<sup>5</sup> The analytic values of  $v_{\max}$  from Eq. (13) agree with those in Table I. The fall-through time was calculated from Eq. (14) for several values of  $n$  using the same 4th-order Runge-Kutta method and they also agreed with the numerical results. Because  $T_0$  depends only on  $n$  and  $\rho_c$ , the fall-through time of any object can be calculated by scaling the values in Table I. The value of  $v_{\max}$  depends on  $R$  as well as  $n$  and  $\rho_c$ , so the physical size must be also specified to calculate the velocity.

The radius and velocity of an object dropped into a tunnel through polytropic models of Earth are shown as a function of time in Fig. 3. You can see that the particle velocities are similar until  $t/T_f \sim 0.6$ . At longer times the models with higher  $n$  diverge from those with lower  $n$  in a regular pattern. This led to an examination of how the velocity varied with radius using the lower half of a phase space diagram (Fig. 4), where the pattern is even more apparent. The motion of the object does not depend on  $n$  when it is moving near the

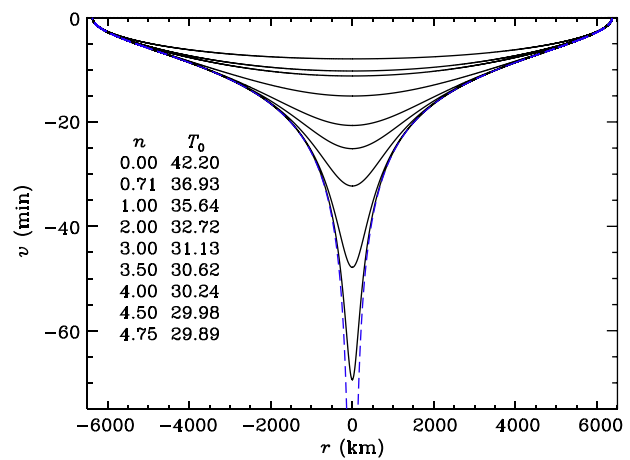


Fig. 4. The lower half of the phase plane of radial position and velocity for an object falling through models of Earth. Values of  $n$  and  $T_0$  are shown in the legend; the solid curves track  $n$  from the top down. The radial free-fall velocity from Eq. (15) is shown as a dashed curve. The calculated velocity is reproduced with a negative radius to better show the variation of the velocity along the entire trajectory from being released on the right to emerging on the other side to the left.

surface. As the object moves closer to the center, it moves much faster in models with higher  $n$ —a demonstration of the law of gravity. In models with larger  $n$ , the peak in  $g$  is deeper inside the model. Because the peak acceleration occurs deeper in the model, the velocity at the center also increases.

The envelope of the calculated infall velocities tracks the radial infall velocity of an object dropped from a distance  $R_{\oplus}$  from a point mass

$$v_{\text{point}} = -\sqrt{\frac{2GM_{\oplus}}{R_{\oplus}} \left( \frac{R_{\oplus}}{r} - 1 \right)} = -11.2 \sqrt{\frac{R_{\oplus}}{r} - 1} \text{ km s}^{-1}. \quad (15)$$

This radial infall velocity is shown as a blue dashed line in Fig. 4.

The time to fall from a distance  $R_{\oplus}$  from a point mass to the center and back to the same distance is

$$T_{0,\text{point}} = \pi \sqrt{\frac{R_{\oplus}^3}{2GM_{\oplus}}} = 29.83 \text{ min}, \quad (16)$$

which is  $\sqrt{2}$  times the uniform-density fall-through time. A point mass represents the limit of ever-increasing mass concentration at the center of our model planet. Thus, this time is a lower limit to the fall-through time and is listed in the last line of Table I. This comparison was also made by Simoson.<sup>25</sup>

The effective size of Earth cannot become smaller than the Schwarzschild radius of about 9 mm, which would imply a radial infall velocity approaching the speed of light. This scenario is not appropriate here so a maximum radial infall velocity is not listed for that case in Table I.

## V. BRACHISTOCHRONES IN POLYTROPES

A tunnel through Earth joining two points on the surface that are not antipodal can be calculated as a brachistochrone, or path of the shortest time, by minimizing the travel time between the two points. These paths were first considered in 1696 by Johann Bernoulli and led to the development of the calculus of variations.

The time to move through any tunnel is the integral along the path between the drop point and where the brachistochrone is tangent to the radius  $R_d$  is

$$\tau = 2 \int_0^{\vartheta(R)} \frac{\sqrt{r^2 d\vartheta^2 + dr^2}}{v(r)} dr, \quad (17)$$

where  $\vartheta$  is the angle between the two points. Klotz<sup>5</sup> showed that the traversal time is minimized when the change in radius per angle is

$$\frac{dr}{d\vartheta} = \frac{r}{R_d} \sqrt{\frac{r^2 I(R_d) - R_d^2 I(r)}{I(r)}}, \quad (18)$$

where the integral  $I(r) = \int_r^R g(r') dr'$  is the change in the potential energy. Using Eq. (9), converting to polytropic coordinates, and canceling constants, this equation becomes

$$\frac{d\xi}{d\vartheta} = \frac{\xi}{\xi_d} \sqrt{\frac{\xi^2 \theta(\xi_d) - \xi_d^2 \theta(\xi)}{\theta(\xi)}}. \quad (19)$$

Substituting the solution for the constant density ( $n=0$ ) polytrope ( $\theta = 1 - \xi^2/\xi_0^2$ ) will recover Eq. (17) of Klotz. By using the polytropes, the integral is simplified by the substitution of  $\theta$  as the gravitational potential while introducing a new class of solutions that smoothly vary with central condensation. This expression can be integrated to give the path parameterized as  $(\xi, \vartheta)$  points

$$\begin{aligned} \vartheta(\xi) &= \int_{\xi_d}^{\xi} \frac{\xi_d}{\xi} \sqrt{\frac{\theta(\xi)}{\xi^2 \theta(\xi_d) - \xi_d^2 \theta(\xi)}} d\xi \\ &= \int_{\xi_d}^{\xi} \sqrt{\frac{\theta(\xi)/\theta(\xi_d)}{(\xi/\xi_d)^2 - \theta(\xi)/\theta(\xi_d)}} \frac{d\xi}{\xi}. \end{aligned} \quad (20)$$

The angle at the surface  $\vartheta(\xi_0)$  is the distance traveled by the tunnel from the surface to the turning point at  $\xi_d$ . Except for the constant density case, the solutions for Eq. (20) using polytropes must be numerically integrated.

The divergence of the integral in Eq. (20) near the turning point at  $\xi = \xi_d$  is handled by expanding the denominator in a Taylor series and analytically integrating the first few points in the curve. Define  $u = \xi/\xi_d$  for  $\xi \geq \xi_d$  and write

$$\begin{aligned} \vartheta_{\text{an}} &= \sqrt{\frac{1}{2 - d\ln\theta/du|_{u=1}}} \int_1^{u_{\text{an}}} \frac{du}{u\sqrt{u-1}} \\ &= \sqrt{\frac{1}{2 - d\ln\theta/du|_{u=1}}} \tan^{-1} \sqrt{u_{\text{an}} - 1}. \end{aligned} \quad (21)$$

The travel time, or the time to takes to move through the tunnel from the entry point to the exit point, is twice the time from the entry point to the turning point

$$\tau = 2 \int_{\text{path}} \frac{\sqrt{dr^2 + r^2 d\vartheta^2}}{v(r)} = 2 \int_{R_d}^R \sqrt{\frac{1 + (r d\vartheta/dr)^2}{2I(r)}} dr. \quad (22)$$

Converting from  $r$  to the polytropic coordinate  $\xi$ , and moving the units outside the integral, the travel time is

$$\tau = \epsilon \sqrt{\frac{2}{4\pi G \rho_c^2}} \int_{\xi_d}^{\xi_0} \sqrt{\frac{1 + (\xi d\vartheta/d\xi)^2}{\theta(\xi)}} d\xi. \quad (23)$$

The next step is to substitute the curvature term in Eq. (19) to get

$$\tau = \sqrt{\frac{1}{2\pi G \rho_c}} \int_{\xi_d}^{\xi_0} \sqrt{\frac{\theta(\xi_d)/\theta(\xi)}{\xi^2 \theta(\xi_d) - \xi_d^2 \theta(\xi)}} \xi d\xi. \quad (24)$$

Defining  $u = \xi/\xi_d$  and  $f = \theta(\xi)/\theta(\xi_d)$ , the integral becomes

$$\tau = \sqrt{\frac{1}{2\pi G \rho_c \theta(\xi_d)}} \xi_d \int_1^{u_0} \frac{u du}{\sqrt{f(u^2 - f)}}, \quad (25)$$

which is the same as the first line of Eq. (6) in Venezian<sup>26</sup> if the  $n=0$  solution is substituted for  $f$ . Equation (25) has divergences at both limits of the integral ( $f=1$  at  $u=1$ ;  $f=0$  at  $u=u_0$ ). These divergences can be overcome by expanding the integrand near the limits and doing the integrals analytically. We thus use  $\tau = \xi_d / \sqrt{2\pi G \rho_c \theta(\xi_d)} (\tau_i + \tau_m + \tau_o)$ , where

$$\begin{aligned}\tau_i &= \sqrt{\frac{1}{2 - d\ln\theta/du}} \int_1^{u_{in}} \frac{u du}{\sqrt{u-1}} \\ &= \sqrt{\frac{1}{2 - d\ln\theta/du}} \frac{2}{3} (u_{in} + 2) \sqrt{u_{in}-1}\end{aligned}\quad (26)$$

for  $u_d = 1 \leq u \leq u_{in}$ ,

$$\tau_m = \int_{u_{in}}^{u_{out}} \frac{u du}{\sqrt{f(u^2 - f)}}\quad (27)$$

for  $u_{in} < u < u_{out}$ , and

$$\begin{aligned}\tau_o &= \sqrt{\frac{1}{-d\ln\theta/du}} \int_{u_{out}}^{u_0} \frac{du}{\sqrt{u_0-u}} \\ &= \frac{2}{\sqrt{-d\ln\theta/du}} \sqrt{u_0-u_{out}}\end{aligned}\quad (28)$$

for  $u_{out} \leq u \leq u_0$ .

Opening angles and travel times were calculated for  $n=0, 1, 2$ , and  $3$  with the three radial distances used in Fig. 6 of Klotz,<sup>5</sup>  $\xi_d/\xi_0 = 0.15, 0.5$ , and  $0.9$ . One trajectory for a turning point distance of  $0.15$  and  $n=4.5$  to show how the continuing concentration of the mass at the center of the model appears to lead to a deflection angle of  $2\pi/3 = 120^\circ$ , similar to a point mass.<sup>10</sup>

The results are summarized in Table II, and the paths are shown in Fig. 5. The paths are reflected about the turning point for a complete journey. The first line of Table II has the opening angles and travel times for the homogeneous sphere.<sup>26</sup> Models with larger  $n$ 's have smaller opening angles for the same radial distance. Larger  $n$  also means a shorter travel time as the larger speeds near the turning point hasten the object along. As expected, the effect of changing the central condensation is smaller for tunnels that stay close to the surface and larger for deeper tunnels.

When comparing models with different values of  $n$ , the identification of angle and  $R_d$  is no longer unique due to the differing central condensations. Although results are reported here with values of  $R_d/R$ , it is as valid to organize

Table II. Opening angles and travel times of Earth-like polytropes.

$\xi_d/\xi_0$	0.15	0.50	0.90	0.15	0.50	0.90
$n$	$\theta$ (deg)			$\tau$ (min)		
0 <sup>a</sup>	153	90	18	41.7	36.6	18.4
0	153	89.9	18.2	40.9	36.6	18.7
1	149	82.3	17.1	33.3	30.4	17.4
2	142	75.1	17.0	29.8	28.0	17.3
3	131	70.7	16.9	28.0	27.1	17.3

<sup>a</sup>Values from solutions of Venezian.<sup>26</sup>

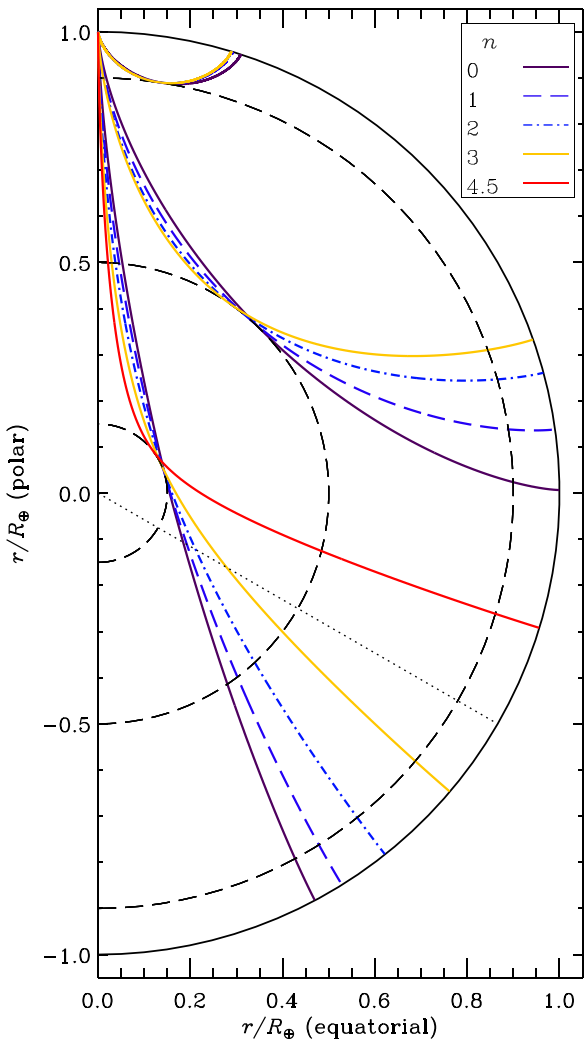


Fig. 5. Brachistochrones for five different polytropes and three different minimum radial distances (only one path is shown for  $n=4.5$ ). All radial positions are normalized by the outer radius. For a given radial distance, a shorter angular distance is traversed when  $n$  is increased. Each end of a brachistochrone intersects the surface at a right angle. Dashed lines are drawn at the selected radial distances, and a solid line is drawn at the surface radius of the model. The dotted line drawn at a colatitude of  $2\pi/3 = 120^\circ$  shows the limiting angle for brachistochrones passing very close to a point mass.

the results by the angle or distance along the surface. If the angle were reported, it would be necessary to iterate on the value of  $R_d$  until the angles matched for the different models.

Brachistochrones can also be calculated for a particle moving in the gravitational field of a point mass.<sup>9</sup> The most significant recent result is an angular range into which the trajectories do not enter as the impact parameter approaches zero.<sup>10</sup> This region extends between  $120^\circ$  and  $180^\circ$  from the entry point. Although the polytropic solutions show a similar avoidance of an angular region, the central pressure and density of an  $n=5$  polytrope are not infinite, as the central condensation diverges because the  $\xi_0$  value extends to infinity. This means that gravity drops to zero at the center of the model and the divergence of the point mass is avoided. As the turning point radius shrinks to zero, the trajectories will eventually probe the region of decreasing gravity and become a tunnel through the object. This behavior is demonstrated in Fig. 6, where the opening angle is shown as a function of  $R_d$  for an  $n=4.5$  polytrope. A linear extrapolation of

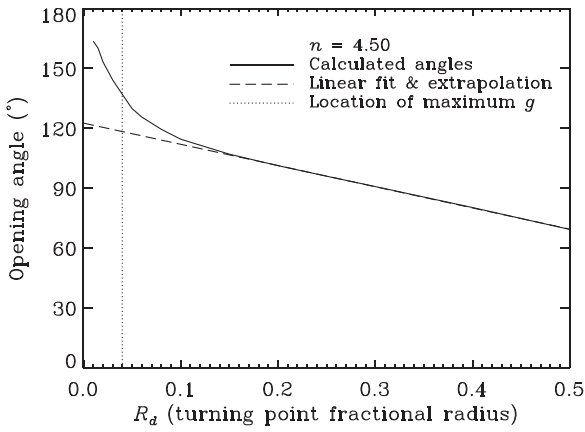


Fig. 6. Opening angle as a function of turning point fractional radius for an  $n=4.5$  polytrope. The solid line shows the calculated opening angles for each value of  $R_d$ . The dashed line is a fit to points with  $0.15 < R_d \leq 0.5$  that is extrapolated to cover the full range of the dependent variable. The vertical dotted line is drawn at the location of the maximum in  $g$ .

the opening angles with  $0.15 < R_d \leq 0.5$  does intersect the  $y$ -axis at about  $120^\circ$ . The peak value of  $g$  is at  $R_d \approx 4 \times 10^{-2}$  [Fig. 1(b)]. Within that radius the trajectories warp back toward a tunnel through the center of the model with an opening angle of  $180^\circ$ .

## VI. GAS GIANTS, WHITE DWARFS, AND DEGENERATE ELECTRONS

Gas giant planets can have degenerate electrons in their cores, which come from the metallic hydrogen formed at the large densities and low temperatures in the core.<sup>13</sup> This region may span a small fraction of the planetary radius, but the degenerate electron pressure is an effective barrier to gravitational settling. Degenerate electrons will also provide pressure sufficient to support the typical star as it evolves into a white dwarf, which has the mass of a star but the size of a planet, even as the internal temperature cools to zero. How fast would an object fall through a pole-to-pole tunnel bored though an object held up by degenerate electrons?

A simple model for white dwarfs assumes a completely degenerate electron gas exists throughout the model, although, in reality, the outermost layers should be nondegenerate. These models are described in Chapter 11 of Chandrasekhar,<sup>18</sup> where they are used to derive a limiting mass for white dwarfs. The fall-through time for a family of completely degenerate objects (CDOs) will be described.

The parametric equation of state for the pressure of completely degenerate electrons is  $P=Af(x)$ , where the parameter  $x$  is related to the density by  $\rho=B\mu_e x^3$ , and the Fermi-Dirac pressure function is

$$f(x) = x(x^2 + 1)^{1/2}(2x^2 - 3) + 3\sinh^{-1}x. \quad (29)$$

The constants are  $A = \frac{\pi}{3}m_ec^2/\lambda_c^3 = 6.002 \times 10^{22} \text{ dyn cm}^{-2}$  and  $B = \frac{8\pi}{3}(\lambda_c^3 N_0)^{-1} = 9.739 \times 10^5 \text{ g cm}^{-3}$ , where  $\lambda_c = h/(m_e c) = 2.4263 \text{ pm}$  is the Compton wavelength of the electron. The dependence of  $x$  on the mean molecular weight per electron ( $\mu_e$ , the number of nucleons per free electron) will be needed below. Instead of a polytropic index, the central value of  $1+x_c^2=y_0^2$  is used as a parameter to describe how relativistic the electrons are in the model. Non-relativistic electrons

correspond to  $y_0^{-2}=1$  and relativistic electron have  $y_0^{-2} \rightarrow 0$ . The central density increases as mass is added to the object and the relativistic parameter  $y_0^{-2}$  decreases from 1 to 0 as the electrons in the core become progressively more relativistic.

Continuing as outlined in Chapter 11 of Chandrasekhar,<sup>18</sup> we introduce a polytropic function  $\phi = (1+x^2)y_0^{-2}$  and a new independent variable that is defined by  $r = \epsilon\eta$ , where

$$\epsilon = \sqrt{\frac{2A}{\pi G}} \frac{1}{\mu_e B} y_0^{-1} = \frac{7.71 \times 10^8}{\mu_e y_0} \text{ cm} = \frac{1.21 R_\oplus}{\mu_e y_0}. \quad (30)$$

Most of the material that would be found in a CDO has  $\mu_e \sim 2$  and  $y_0^{-2}$  ranges from 0 to 1. Therefore, all objects supported by completely degenerate electrons are the size of planets.

The transformed equation of hydrostatic equilibrium [Eq. (1)] becomes

$$\frac{1}{\eta^2} \frac{d}{d\eta} \left( \eta^2 \frac{d\phi}{d\eta} \right) = - \left( \phi^2 - y_0^{-2} \right)^{3/2}, \quad (31)$$

which has a solution requiring two boundary conditions that are chosen as  $\phi = 1$  and  $d\phi/d\eta = 0$  at  $\eta = 0$ . The surface of the model is at the first point where  $\phi^2 = y_0^{-2}$ .

Completely degenerate objects behave like polytropes at both limits of  $y_0^{-2}$ . The effective polytropic index changes from  $n=1.5$  for  $y_0^{-2} \rightarrow 1$  (radius decreases with increasing mass) to  $n=3$  for  $y_0^{-2} \rightarrow 0$  (mass and radius are not coupled).

The variation of mass density with radius of CDOs with  $0.01 \leq y_0^{-2} \leq 0.99$  was calculated by integrating Eq. (31) from the core to the surface of the model<sup>23,24</sup> and using a shooting method to converge  $\eta_0$ . The results are summarized in Table III, the first six columns of which can be compared to Table 25.1 in Ref. 12. The most important feature is how the physical radius in column 6 shrinks as  $y_0^{-2}$  becomes small. The polytropic radius in column 2 ( $\eta_0$ ) does not tend toward zero, but the physical size of the CDO does. This leads to the maximum mass of a CDO.<sup>18</sup> Normal white dwarfs have  $\mu_e \approx 2$  (each electron is associated with the mass of one proton and one neutron) and a limiting mass of approximately  $1.4 M_\odot$ .

Unlike the polytropes, it is not possible to build a CDO model with a chosen mass *and* radius. While these models assume  $\mu_e = 1$ ,  $\mu_e$  could be adjusted to make all of the models have the same radius, though this would come at the expense of the mass, which can be seen by adjusting the radius of the limiting mass as  $y_0^{-2} \rightarrow 0$ . Changing  $\mu_e$  to make the radius of the  $y_0^{-2} = 0.01$  object equal to  $R_\oplus$  means that  $\mu_e = 4133/6371 = 0.649$  and the mass would be  $M_\odot/\mu_e^2 = 5.58/0.649^2 \approx 13.3 M_\odot$ .

Column 7 of Table III lists the values of  $T_0$ , found by integrating the free-fall equation of motion from the surface to the core and multiplying by two. White dwarfs have much higher surface gravity than a regular star of the same mass or Earth (which has a similar radius). As a result  $T_0$  for white dwarfs is much shorter and  $v_{\max}/c$  (the 8th column) is much larger than for a model of Earth. Classical mechanics was used throughout the calculations, so relativistic corrections were not included. Although the relativistic corrections for  $v_{\max}/c \sim 0.1$  are not that large, further decreases in  $y_0^{-2}$  below 0.01 should probably include those effects. The variations of  $T_0$  and  $v_{\max}/c$  with  $y_0^{-2}$  are shown in Fig. 7.

Table III. Properties of Completely Degenerate Objects.<sup>a</sup>

$y_0^{-2}$	$\eta_0$	$-\eta_0^{2d\phi}/d\eta _0$	$\rho_c/\bar{\rho}$	$M^\circ (M_\odot)$	$R^\circ (\text{km})$	$T_0 (\text{min})$	$v_{\max}/c$
Extremely Relativistic							
0.01	5.357	1.932	26.132	5.58	4133	0.0171	0.0997
0.02	4.986	1.865	21.488	5.39	5439	0.0239	0.0819
0.05	4.460	1.710	16.018	4.94	7693	0.0401	0.0619
0.10	4.069	1.519	12.629	4.39	9926	0.0592	0.0489
0.20	3.727	1.243	9.937	3.59	12858	0.0933	0.0370
0.30	3.580	1.034	8.666	2.99	15127	0.1287	0.0302
0.50	3.533	0.707	7.351	2.04	19271	0.2207	0.0214
0.80	4.045	0.309	6.382	0.89	27906	0.5748	0.0114
0.90	4.696	0.177	6.171	0.51	34362	1.0351	0.0077
0.99	8.187	0.030	6.008	0.088	62838	6.1449	0.0024
Non-Relativistic							

<sup>a</sup>Values of  $T_0$ , and  $v_{\max}$  were calculated for  $M = M^\circ / \mu_e^2$ ,  $R = R^\circ / \mu_e$ , and  $\mu_e = 1$ .

The extrapolated result for an  $n=3$  polytrope, scaled to the CDO density, is shown as a filled circle on the  $y_0^{-2} = 0.01$  axis. Similarly, an  $n=1.5$  polytrope is on the  $y_0^{-2} = 1$  axis. The latter value is steeply sloped as  $y_0^{-2} \rightarrow 1$  but the  $y_0^{-2} = 0.99$  model agrees well with the  $n=1.5$  polytrope scaled to the same mass and radius. In the relativistic limit, the approach to the  $n=3$  polytrope is much slower and a value  $y_0^{-2} = 10^{-6}$  is needed to reach this limit. While polytropes can be used to estimate  $T_0$  at the limits, the intermediate values of  $y_0^{-2}$  are not polytropes and cannot be analyzed in this fashion. However, the brachistochrones for CDOs were not displayed as they do not differ greatly from the polytropes results presented earlier unless relativistic effects are considered.

Figure 7 shows that there is no simple scaling of  $T_0$  with  $y_0^{-2}$ . The scaling of  $T_0$  with  $\mu_e$  is  $T_0 \sim \mu_e^{-1/2}$  (at constant  $y_0^{-2}$ ). Typical white dwarfs have  $\mu_e \approx 2$ , and the values of  $T_0$  in Table III must be multiplied by  $\sim 0.71$  to represent models with that composition.

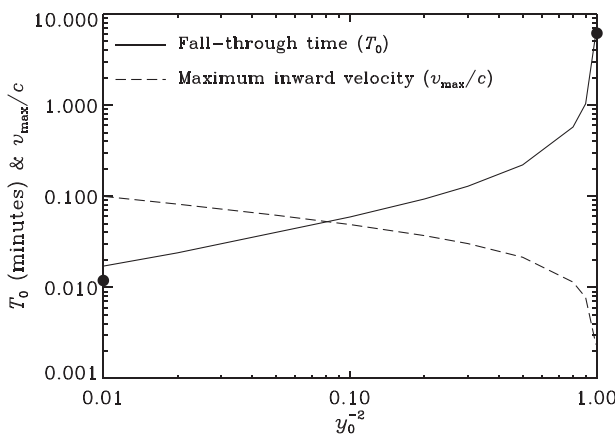


Fig. 7. Fall-through time and maximum inward velocity as a function of the relativistic parameter  $y_0^{-2}$  for completely degenerate objects. The solid line shows the calculated fall-through times, and the dashed line is the velocity as listed in Table III. Extrapolating to the limiting  $n=3$  polytropes for relativistic CDOs gives the scaled value  $T_0(n=3) = 1.30 \times 10^{-2} \text{ min}$  (closed circle on left axis). An extrapolation to the non-relativistic limit of an  $n=1.5$  polytrope is sensitive to the last value of  $y_0^{-2}$  used as the scaling density. For  $y_0^{-2} = 0.99$  the scaling is  $\sqrt{5.514/168.4}$  and gives  $T_0(n=1.5) = 6.15 \text{ min}$  (closed circle on right axis).

## VII. CONCLUSIONS

We have shown that polytropes offer a way to calculate the fall-through time of models of Earth that have varying central condensations. We used those polytropes to link the fall-through time of Earth with the free-fall time to a point mass, which provides a lower limit for the fall-through time that is otherwise not accessible. We also showed that the fall-through times are much shorter for the completely degenerate objects, which are Earth-sized but have masses similar to the Sun. The maximum infall velocity of CDO's can become relativistic. We have also provided a way to link models of planets to models of stars by looking at how the variation of the interior gravity changes the motions of particles falling through the models.

The calculation of brachistochrone paths through Earth that connect surface points that are not antipodal may have other uses. These paths were calculated by several authors as transportation methods<sup>1,5,15–17</sup> and were the original inspiration for considering these tunnels.<sup>4</sup> These brachistochrones resemble the acoustic ray travel paths for oscillations of solar models shown in Fig. 4 of the review paper by Christensen-Dalsgaard.<sup>27</sup> The mathematics is almost identical, although the oscillations use the horizontal and radial wave numbers in the integrals for the opening angle [Eq. (20)] and travel time [Eq. (22)]. The turning points have the same integrable divergences as described here. Although a proof of their equivalence was not demonstrated here, there may be a connection that makes the study of tunnels in planets relevant to the oscillations of planets and stars.

Both the maximum velocity of the fall-through tunnel and the “shortest time” paths were shown to be simplified when using polytropes within the formalism of Klotz,<sup>5</sup> because the polytropic function is the gravitational potential the formalism requires. The angular distance traveled is smaller for a given radial distance at larger  $n$ , and the travel time is shorter. Both of these effects are smaller as the radial distance approaches the surface.

Imagining tunnels through Earth forces us to come up with a way to analyze a new situation. In this case, a system has simple harmonic motion similar to springs and pendula even though it looks nothing like those everyday devices. That something could fall through Earth, reaching orbital velocities at the midpoint, but then pause at the antipodal point to be plucked from the opening can speak to a student

in ways that a primitive apparatus cannot. That it could be envisioned for other objects might help the students to better use those interior models. It is also important that other concepts can flow from this simple experiment. Trains running through tunnels are a natural next step, and the internal motions of the planets, either from thermal convection or earthquakes, are another. The magnitude of orbital velocities can also be motivated by combining this experiment with Newton's cannon. Abstract thought is an important part of the undergraduate physics curriculum, and tunnels through planets are a potential step toward developing those thought processes.

These examples may also provide the knowledge needed to overcome the misinterpretation of scientific results when used to draw the wrong conclusions. Soon after the publication of the letter of Redier,<sup>4</sup> a short article appeared in the *New York Times*<sup>28</sup> that announced "To Rio de Janeiro in Two Hours." Unfortunately, they were referring to a telegraph signal and the two hour interval was due to the differing timezones of the two cities.

## ACKNOWLEDGMENTS

The authors gratefully acknowledge the support of NASA's Solar Dynamics Observatory. The comments of the referees were useful in clarifying the discussion of the fall-through time calculation.

## APPENDIX: SAMPLE QUESTIONS AND EXERCISES

To help illustrate the usefulness of these simplified models to the study of planets and stars, the following questions would encourage students to use the tabulated results to explore other planets:

- (1) Calculate the fall-through time for other planets in two different ways. First, scale the results from Table I to have the same mass and radius as the other planets in the solar system. Second, integrate the equations of motion using the gravity of  $n=0$  and 1 polytropes (which have closed-form solutions) scaled to represent the other planets.
- (2) Calculate the fall-through time for completely degenerate objects scaled to have the same radius as the planets in two different ways. You can scale both the  $T_0$  and  $v_{\max}$  results from Table III to have the radius of the planets in the solar system. What is the mass of these CDOs (in solar masses)? How long would it take to fall through each of those objects?
- (3) The original Standard Model of the Sun was an  $n=3$  polytrope. Using Table I, what is the fall-through time for that model? Compare these times with the orbital period of a satellite in a circular orbit at the surface of Earth and the Sun.
- (4) What force must be applied to keep the object moving along the path of the brachistochrones? This can be evaluated by considering the normal force in the body frame. The force can be provided by a rail along the wall of the tunnel inside a terrestrial planet but flying through a gas giant would require a propulsion system.
- (5) Plot the integrands of Eqs. (20) and (25) and show the region where the divergence can be removed by using the expansions near the integration limits. These types of

integrals are common when inverting satellite data, especially radiances measured at the limb of Earth and other planets.<sup>29–31</sup> Radiances are the measured brightnesses referenced to the closest distance the line of sight passes to the planet, which is called the tangent point and corresponds to  $R_d$  in this discussion. Because the instrument looks through the atmosphere above the tangent point, it is necessary to account for that emission when inverting the data to determine the temperature and composition of the atmosphere.

- (6) What would be different if a neutron star could be tunneled through? Polytropic solutions to the Tolman-Oppenheimer-Volkoff equations are described in Tooper.<sup>32</sup> A relativistic degenerate neutron equation of state is used in these models, which limits their accuracy. What equations must be integrated to calculate the fall-through time in these models?

<sup>a)</sup>Electronic mail: William.D.Pesnell@NASA.gov

<sup>1</sup>P. W. Cooper, "Through Earth in forty minutes," *Am. J. Phys.* **34**(1), 68–70 (1966).

<sup>2</sup>P. G. Kirmser, "An example of the need for adequate references," *Am. J. Phys.* **34**(8), 701–701 (1966).

<sup>3</sup>C. W. Misner, K. S. Thorne, and J. A. Wheeler, *Gravitation* (W. H. Freeman, San Francisco, 1973).

<sup>4</sup>A. Redier, "De Paris à Rio de Janeiro en 42 minutes et 11 secondes," *La Nature* (1883); available at <http://sciences.globik.info/spip.php?article1223>.

<sup>5</sup>A. R. Klotz, "The gravity tunnel in a non-uniform Earth," *Am. J. Phys.* **83**(3), 231–237 (2015).

<sup>6</sup>The inward velocity of a particle approaching a mass from far away. The escape velocity is the velocity at the surface of the planet required to move far from the planet and corresponds to the negative of the radial infall velocity at the surface.

<sup>7</sup>A. R. Klotz, "A guided tour of planetary interiors," e-print [arXiv:1505.05894](https://arxiv.org/abs/1505.05894) [physics.pop-ph], version dated 18 May 2015 accessed on 23 Sep. (2015).

<sup>8</sup>W. D. Pesnell and P. Bryans, "The time-dependent chemistry of cometary debris in the solar corona," *Astro. Phys. J.* **785**, 50–1–50–10 (2014).

<sup>9</sup>E. J. Routh, *A Treatise on Dynamics of a Particle* (Cambridge U.P., Cambridge, 1898), accessed as <<https://ia700406.us.archive.org/28/items/atreatiseondyna03routgoog/atreatiseondyna03routgoog.pdf>>.

<sup>10</sup>G. J. Tee, "Isochrones and brachistochrones," *Int. Conf. Neural Parallel Sci. Comput.* **7**(3), 311–341 (1999).

<sup>11</sup>A. S. Eddington, *Internal Constitution of Stars* (Cambridge U.P., Cambridge, 1926).

<sup>12</sup>J. P. Cox and R. T. Giuli, *Principles of Stellar Structure*. (Gordon & Breach, New York, 1968).

<sup>13</sup>B. Militzer and W. B. Hubbard, "Ab initio equation of state for Hydrogen-Helium mixtures with recalibration of the giant-planet mass-radius relation," *Astro. Phys. J.* **774**, 148–1–148–11 (2013).

<sup>14</sup>D. Saumon, G. Chabrier, and H. M. van Horn, "An equation of state for low-mass stars and giant planets," *Astro. Phys. J. Suppl.* **99**, 713–741 (1995).

<sup>15</sup>P. W. Cooper, "Further commentary on 'Through Earth in Forty Minutes,'" *Am. J. Phys.* **34**(8), 703–704 (1966).

<sup>16</sup>L. Jackson Laslett, "Trajectory for minimum transit time through Earth," *Am. J. Phys.* **34**(8), 702–703 (1966).

<sup>17</sup>R. L. Mallett, "Comments on 'Through Earth in Forty Minutes,'" *Am. J. Phys.* **34**(8), 702–702 (1966).

<sup>18</sup>S. Chandrasekhar, *An Introduction to the Study of Stellar Structure* (Dover, New York, 1967).

<sup>19</sup>The Extrasolar Planets Encyclopaedia website (<<http://exoplanet.eu>>) now lists over 1950 extrasolar planets.

<sup>20</sup>J. J. Lissauer, "Kepler: A giant leap for exoplanet studies," *EOS* **96**, 12–17 (2015).

<sup>21</sup>A. M. Dziewonski and D. L. Anderson, "Preliminary reference Earth model," *Phys. Earth Plan. Int.* **25**, 297–356 (1981).

<sup>22</sup>The PREM model was downloaded as PREM500.csv from <<http://ds.iris.edu/ds/products/emc-prem/>>.

<sup>23</sup>W. D. Pesnell, "Weight functions in adiabatic stellar pulsations. I-Radially symmetric motion," *PASP* **99**, 975–985 (1987).

- <sup>24</sup>W. D. Pesnell, "Properties of Eötvös spheres," *Astro. Phys. J.* **344**, 851–855 (1989).
- <sup>25</sup>A. J. Simoson, "The gravity of Hades," *Math. Mag.* **75**(5), 335–350 (2002).
- <sup>26</sup>G. Venezian, "Terrestrial brachistochrone," *Am. J. Phys.* **34**(8), 701 (1966).
- <sup>27</sup>J. Christensen-Dalsgaard, "Helioseismology," *Rev. Mod. Phys.* **74**, 1073–1129 (2002).
- <sup>28</sup>New York Times, "To Rio de Janeiro in Two Hours," 1883.
- <sup>29</sup>C. R. Chester, *Techniques in Partial Differential Equations* (McGraw-Hill, New York, 1971).
- <sup>30</sup>P. B. Hays and R. G. Roble, "Atmospheric properties from the inversion of planetary occultation data," *Planet. Space Sci.* **16**, 1197–1198 (1968).
- <sup>31</sup>P. B. Hays and R. G. Roble, "Stellar spectra and atmospheric composition," *J. Atmos. Sci.* **25**, 1141–1153 (1968).
- <sup>32</sup>R. F. Tooper, "General relativistic polytropic fluid spheres," *Astro. Phys. J.* **140**, 434–459 (1964).



**Figure of the Earth Demonstration**

We tell students that the earth is an oblate spheroid, flattened at the poles. Earlier students saw this flattening for themselves by using this Figure of the Earth demonstration. The spring brass strips are attached to the shaft at the top, but the bottom ends are free to ride up and down on the shaft. In the latter part of the 19<sup>th</sup> century this apparatus cost about \$3.00. It is in the Greenslade Collection. (Notes and picture by Thomas B. Greenslade, Jr., Kenyon College)